Grid Impedance Identification and Structured-h2 Optimization Based Controller Design of Active Front-end in Embedded AC Networks

Kang Li,David Dewar,Andrea Formentini,Pericle Zanchetta and Pat Wheeler
Power Electronics,Machines and Control Group
University of Nottingham,Nottingham,UK
Email:kang.li@nottingham.ac.uk

***Abstract*—The increasing use of power electronics systems and distributed generation in modern power networks has raised important issues regarding the effects that inter-connected converters systems can have on the performance and stability of the whole grid. Interactions between locally optimized converters, designed not taking into account the external influence of the system in which they are operating, may lead to performance degradation or even system instability and failure. This paper will deal with the problem of active-front end control design taking into account of system interactions with other power converters in the grid. A globally optimized local converter control tuning method, which is based on a state space model identification of the unknown grid system seen from the converter at its point of common coupling (PCC), is here proposed. The plant for the control design will then be not only represented by the local converter dynamics, but will also include the identified system at the PCC. In order to describe and validate the concept, a simplified notional system, comprising of two interconnected converter systems coupled on the same AC bus is analyzed. The effectiveness and advantages of the proposed method is validated by experiments with a traditionally designed PI controller for comparison.**

***Index Terms*—identification, h2 optimization, active front-end**

I. Introduction

Power electronic embedded distributed power systems are being adopted in an increasing number of modern applications, ranging from large energy systems to micro-grids, from the more-electric aircraft to new naval ships power systems [1]. Concerns about performance, power quality and stability of these inter-connected power converters systems, due to the interactions among converters, have arisen, which necessitates of coordinated and optimized control both at converter and at system level.

Such power systems are composed of different types of power converters, which in practice may come from different vendors. Information on commercial products are usually not totally accessible, thus preventing engineers from having a full knowledge of said converters. The lack of accurate mathematical models for all systems in the grid is an obstacle to implement a local control that integrates grid interactions for optimized performance. Especially, when design a controller of an active front-end for a DC load to be attached on a weak ac grid, it is challenging to find a stable and fast controller using traditional PI method. Thus, in order to implement globally optimized control for the local converter, an active front-end in this paper, there is the need to identify a model of the system with unknown parameters seen at the converter PCC.

Theory and implementation of model identification have been well researched to deal with situations where an accurate mathematical model is not available. Algorithms such as the least square method, maximum likelihood method and subspace identification algorithm have been extensively studied [2]. The best approach to estimate a network equivalent model seen by the converter PCC is to operate a grid impedance measurement from the converter itself. In the past considerable research activities were focused on measuring small-signal impedances of power converters and/or systems by perturbation injection and frequency sweeping. These researches aimed to obtain impedance models to aid stability analysis through Nyquist admittance ratio criterion. While in this paper, time-domain response data is gathered in an identification experiment to estimate a state space model of the grid seen at the PCC, which will be integrated in the local converter controller design.

In this paper, an optimized controller tuning method for power converters integrating a grid state space model identification is proposed. It is capable of fine tuning a controller considering interactions between the "to be designed" converter and other converters (with unknown parameters and controllers) connected to the same network. Based on the identified model of the unknown converters, an overall model of the inter-connected converter system is built, by which an optimized controller for the "to be designed" converter is synthesized through structured h2 optimization algorithm achieving optimal control and better dynamic performance. A reduced notional system, including two interconnected converter systems coupled on the same AC bus has been built to demonstrate the validity of proposed approach.

II. VSI-AFE System Model

A schematic of the notional system discussed in this paper is depicted in Fig.1. The ac grid is generated by an off-the-

shelf voltage source inverter (VSI) with an LCR output filter. A constant power load (CPL) fed by an AFE is attached on the grid. An inductive input filter, capacitor output filter and phase-locked loop (PLL) for AFE are included. The optimal control design method proposed will be applied to the AFE.

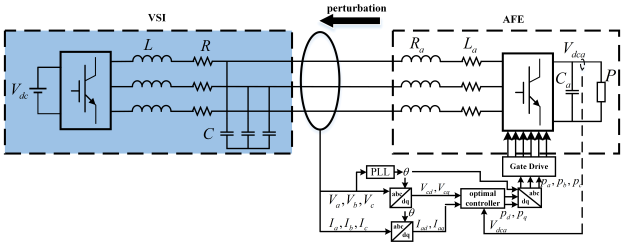

Fig. 1. Schematic of the VSI-AFE notional system

A. Small Signal Model of VSI, AFE and PLL

The current and voltage dynamics of the two subsystems are modelled by (1) and (2) in the dq frame that rotates synchronously with the VSI output voltage angular speed ω [5] [6]. In the case of this study, $\omega = 2\pi \cdot 400$ rad/s. The two subsystems interact through the currents and voltages on the ac bus, represented by $I_{ad/aq}$ and $V_{cd/cq}$, at the PCC.

$$\dot{V}_{cd} = \frac{1}{C} I_{id} + \omega V_{cq} - \frac{1}{C} I_{ad} \tag{1a}$$

$$\dot{V}_{cq} = -\omega V_{cd} + \frac{1}{C} I_{iq} - \frac{1}{C} I_{aq} \tag{1b}$$

$$\dot{I}_{id} = -\frac{R}{L} I_{id} - \frac{1}{L} V_{cd} + \omega I_{iq} + \frac{V_{dc}}{2L} m_d \tag{1c}$$

$$\dot{I}_{iq} = -\omega I_{id} - \frac{R}{L} I_{iq} - \frac{1}{L} V_{cq} + \frac{V_{dc}}{2L} m_q \tag{1d}$$

$$\dot{I}_{ad} = \frac{V_{cd}}{L_a} - \frac{R_a}{L_a} I_{ad} + \omega I_{aq} - \frac{V_{dca} p_d}{2L_a} \tag{2a}$$

$$\dot{I}_{aq} = \frac{V_{cq}}{L_a} - \omega I_{ad} - \frac{R_a}{L_a} I_{aq} - \frac{V_{dca} p_q}{2L_a} \tag{2b}$$

$$\dot{V}_{dca} = \frac{3}{4C_a}(p_d I_{ad} + p_q I_{aq}) - \frac{P}{C_a V_{dca}} \tag{2c}$$

The terms $V_{cd/cq}$ and $I_{id/iq}$ represent the dq-frame VSI output capacitor voltages and inductor currents respectively. $I_{ad/aq}$ and V_{dca} are input filter dq frame currents and output DC-link voltage of the AFE respectively. $m_{d/q}$ and $p_{d/q}$ are the modulation indexes of VSI and AFE respectively. V_{dc} is the DC voltage source of VSI. The passive components R, L and C represent the VSI filter resistance, inductance and capacitance respectively. R_a, L_a represent AFE ac filter resistance, inductance respectively while C_a is AFE output filter capacitance. P represents the power of the CPL.

$$\theta_e = \theta - \theta_0 \tag{3}$$

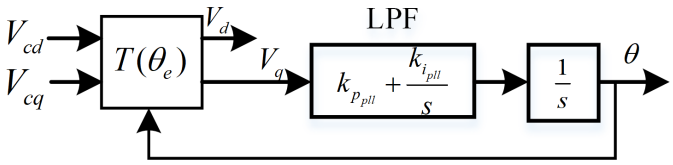

Fig. 2. Block diagram of the SRF-PLL

$$T(\theta_e) = \begin{bmatrix} cos(\theta_e) & sin(\theta_e) \\ -sin(\theta_e) & cos(\theta_e) \end{bmatrix} \tag{4}$$

$$\begin{cases} \dot{\theta}_e = -k_{p_{pll}} V_{cd} \theta_e + x \\ \dot{x} = -k_{i_{pll}} V_{cd} \theta_e \end{cases} \tag{5}$$

The most common PLL is SRF (Synchronous reference frame)-PLL shown in Fig.2. θ_0 is real phase angle of the grid and θ is the identified angle by PLL. Dynamics of the PLL can be modelled by (5) [6]. θ_e is the difference between θ_0 and θ. $k_{p_{pll}}$ and $k_{i_{pll}}$ are the proportional and integral gains of PLL's low pass filter (LPF). x is the output of first integrator with integral gain of $k_{i_{pll}}$.

B. AFE and PLL State Space Model

The linearised state space representation of the AFE is (6):

$$\begin{cases} \dot{x}_{afe} = A_{afe} x_{afe} + B_{afe} u_{afe} + G_{afe} d_{afe} \\ y_{afe} = C_{afe} x_{afe} \end{cases} \tag{6}$$

where

$$x_{afe} = \begin{bmatrix} I_{ad} & I_{aq} & V_{dca} & w_{i_{aq}} & w_{v_{dca}} \end{bmatrix}^T, y_{afe} = \begin{bmatrix} I_{ad} & I_{aq} \end{bmatrix}^T \tag{7}$$

$$A_{afe} = \begin{bmatrix} -\frac{R_a}{L_a} & \omega & -\frac{p_d^*}{2L_a} & 0 & 0 \\ -\omega & -\frac{R_a}{L_a} & -\frac{p_q^*}{2L_a} & 0 & 0 \\ \frac{3p_d^*}{4C_a} & \frac{3p_q^*}{4C_a} & \frac{P}{C_a V_{dca}^2} & 0 & 0 \\ 0 & -1 & 0 & 0 & 0 \\ 0 & 0 & -1 & 0 & 0 \end{bmatrix} \tag{8}$$

$$B_{afe} = \begin{bmatrix} -\frac{V_{dca}}{2L_a} & 0 \\ 0 & -\frac{V_{dca}}{2L_a} \\ \frac{3I_{ad}^*}{4C_a} & 0 \\ 0 & 0 \\ 0 & 0 \end{bmatrix}, G_{afe} = \begin{bmatrix} \frac{1}{L_a} & 0 \\ 0 & \frac{1}{L_a} \\ 0 & 0 \\ 0 & 0 \\ 0 & 0 \end{bmatrix} \tag{9}$$

$$C_{afe} = \begin{bmatrix} 1 & 0 & 0 & 0 & 0 \\ 0 & 1 & 0 & 0 & 0 \end{bmatrix} \tag{10}$$

$$u_{afe} = \begin{bmatrix} p_d & p_q \end{bmatrix}^T, \quad d_{afe} = \begin{bmatrix} V_{cd} & V_{cq} \end{bmatrix}^T \tag{11}$$

$w_{i_{aq}}$ and $w_{v_{dca}}$ are integral states used to eliminate steady state error of the regulated I_{aq} and V_{dca}. I_{aq} is controlled to zero to maintain a unity power factor on the ac bus. The terms with $*$ superscripts in (10) are equilibrium point values of the corresponding states. (12) is the state space representation of the PLL and u_{pll} is virtual input helping to construct state space equations from (5) and has no physical meanings.

$$\dot{x}_{pll} = A_{pll}x_{pll} + B_{pll}u_{pll} \tag{12}$$

$$x_{pll} = \begin{bmatrix}\theta_e & x\end{bmatrix}^T, A_{pll} = \begin{bmatrix}0 & 1\\ 0 & 0\end{bmatrix}, B_{pll} = \begin{bmatrix}-V_{cd} & 0\\ 0 & -V_{cd}\end{bmatrix} \tag{13}$$

$$u_{pll} = k_{pll}x_{pll} = \begin{bmatrix}k_{p_{pll}} & 0\\ k_{i_{pll}} & 0\end{bmatrix}\begin{bmatrix}\theta_e\\ x\end{bmatrix} \tag{14}$$

III. Control design of AFE

In this part, the proposed optimal controller design method for the AFE will be presented and compared with the traditional PI method. The performance of controllers designed in these two different ways will be compared later. Firstly, the control scheme of VSI for the comparison experiment is presented.

In this paper, the VSI is implemented to emulate the grid side system. It is assumed to be unknown for engineers when they do the control design for an converter-interfaced load to be attached on the grid afterwards. Without loss of generality, a traditional cascade PI controller is employed for VSI in this paper. The tuning methods of the PI parameters in such applications are well documented [7] [8].

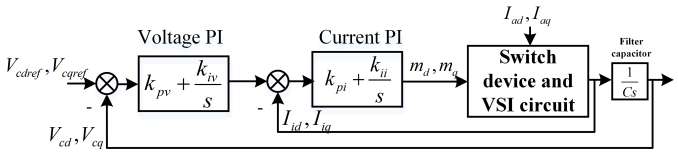

Fig. 3. PI control loop for VSI

$$\begin{cases}\dot{x}_{vsi} = A_{vsi}x_{vsi} + B_{vsi}u_{vsi}\\ y_{vsi} = C_{vsi}x_{vsi}\end{cases} \tag{15}$$

$$u_{vsi} = \begin{bmatrix}I_{ad} & I_{aq}\end{bmatrix}^T, \quad y_{vsi} = \begin{bmatrix}V_{cd} & V_{cq}\end{bmatrix}^T \tag{16}$$

The input-output characteristics of VSI seen from the rest of grid can be fully modelled by the state space model represented by (15). $A_{vsi} \in \mathbb{R}^{m\times m}$,$B_{vsi} \in \mathbb{R}^{m\times 2}$ and $C_{vsi} \in \mathbb{R}^{2\times m}$ are the state matrix, input matrix and output matrix respectively. m is the order of VSI. In actual fact, the existence of this model does not depend on the control scheme the VSI has adopted.

A. Traditional PI Control Design of AFE

The most common control method used is the PI control scheme shown in Fig.4. The sections attribute to dashed lines are only valid in the identification procedure and will be detailed later. The PI gains are tuned by the pole-placement approach (17) [8]. f_i, f_v, and ξ are current, voltage bandwidth and damping factor respectively.

$$\begin{cases}k_{pv} = 2C_a \cdot 2\pi f_v;\\ k_{iv} = C_a \cdot (2\pi f_v)^2;\\ k_{pi} = -2\xi L_a \cdot 2\pi f_i + R_a;\\ k_{ii} = -L_a \cdot (2\pi f_i)^2;\end{cases} \tag{17}$$

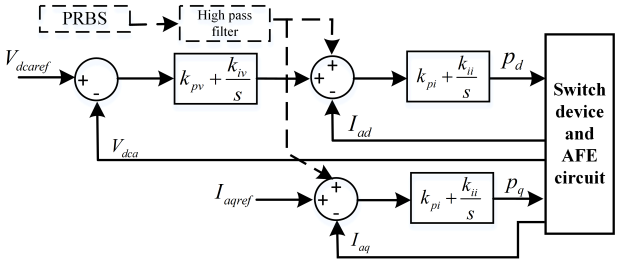

Fig. 4. Traditional PI control loop for AFE

B. Optimal H2 Control Design of AFE

In practice, different parts (sources and loads) of a complex power electronics embedded network may come from different manufacturers and suppliers. They are usually designed and optimized individually at the subsystem level. The dynamics of the grid is not considered and utilized in control design procedure of a local converter. In fact, it will be demonstrated in this paper that if model of the grid can be integrated into the controller design of the AFE, the dynamic response and stability margin of the whole system can be greatly improved. This relies on a full model of the whole system (VSI-AFE system shown in Fig.1), shown in (18).

$$\begin{bmatrix}\dot{x}_{vsi}\\ \dot{x}_{afe}\\ \dot{x}_{pll}\end{bmatrix} = \begin{bmatrix}A_{vsi} & \tilde{B}_{vsi} & \mathbf{0}\\ \tilde{G}_{afe} & A_{afe} & \mathbf{0}\\ \mathbf{0} & \mathbf{0} & A_{pll}\end{bmatrix}\begin{bmatrix}x_{vsi}\\ x_{afe}\\ x_{pll}\end{bmatrix} + \begin{bmatrix}\mathbf{0} & \mathbf{0}\\ B_{afe} & \mathbf{0}\\ \mathbf{0} & B_{pll}\end{bmatrix}\begin{bmatrix}u_{afe}\\ u_{pll}\end{bmatrix} \tag{18}$$

$$\tilde{G}_{afe} = G_{afe}C_{vsi} \tag{19}$$

$$\tilde{B}_{vsi} = B_{vsi}C_{afe} \tag{20}$$

The bold zero matrix are of proper dimensions. In (18), the closed-loop model of VSI shown in (15), is combined with open loop model of to be designed AFE (shown in (6)) and PLL (5). In this way, a full model of the VSI-AFE system is built. It can be used to synthesise a controller for AFE and it inherently has taken into account interactions between the two subsystems. The interactions are expressed as grid voltages V_{cd}, V_{cq} and currents I_{ad}, I_{aq} and take effect by $\tilde{G}_{afe}$ and $\tilde{B}_{vsi}$. The definitions of $\tilde{G}_{afe}$ and $\tilde{B}_{vsi}$ are shown in (19) and (20).

By use of the structured H2-optimization algorithm [9], a controller K can be synthesised and forced with the specified structure S (21) meanwhile. The **1**s are all-ones matrices. Zero matrices in S indicate that corresponding entries of K (namely, controller gains) are zeros. In this way, the controller developed for AFE is independent from state variables of VSI.

$$S = \begin{bmatrix}\mathbf{0} & \mathbf{1} & \mathbf{0}\\ \mathbf{0} & \mathbf{0} & \mathbf{1}\end{bmatrix} \tag{21}$$

The method relies on a model of VSI, which, however, is usually not available in practise. This necessitates identification techniques to be employed to identify a model of VSI.

C. VSI Model Identification

No change of the system hardware configuration is needed in identification experiment. In this case, AFE acts as a current perturbation source. It receives pseudo random binary sequence (PRBS) signals as its current reference, and adds them into the current control loop, shown in the dashed line area in Fig.4. The PRBS signals may need to be filtered to ensure disturbances of equal power across the desired frequency range of interest. The output perturbation currents of the AFE, are injected into the VSI output terminals, and voltage response of the VSI is then sampled. The data of all the analysed currents and voltages are collected and then passed into the Subspace Identification Algorithms (SIA) and Prediction Error Minimization Algorithm. The result is the identified state space model of VSI in the form shown in (15). The model order is selected during the SIA state-space model synthesis according to the Hankel matrix [10].

Validity of the identified model could be checked by comparing bode diagrams of the identified model and the known nominal model. The latter is based on actual parameters used in the rig. In this research, the bode plots of the identified VSI model match those of the nominal model, comfortably in the frequency range of interest, which means the identified model describes the real dynamic behaviour of VSI well. It could also be seen later that the optimal H2 controller designed by this identified model achieved a good performance. This identified model will be utilized to replace (15) in building system overall model (18).

IV. Performance Comparison and Anylysis of Optimal H2- and Traditional PI Controller

To investigate the effectiveness of the proposed optimal controller design method, an experimental setup has been built, shown in Fig.5. Passive components and reference values are shown in Table.I.

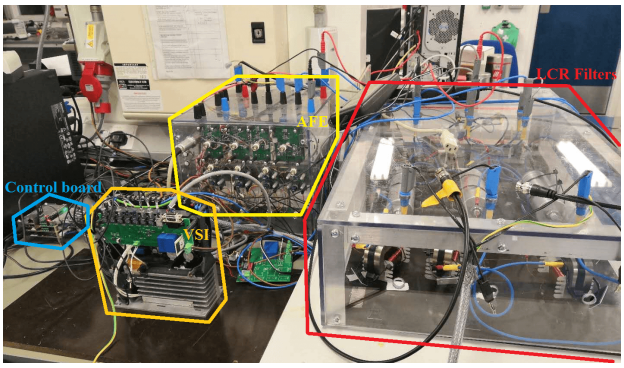

Fig. 5. Experimental rig of the VSI-AFE system

A. Case with Higher Bandwidth VSI

In the first case, a VSI is employed with traditional PI controller with parameters shown in the 2nd row of Table.II

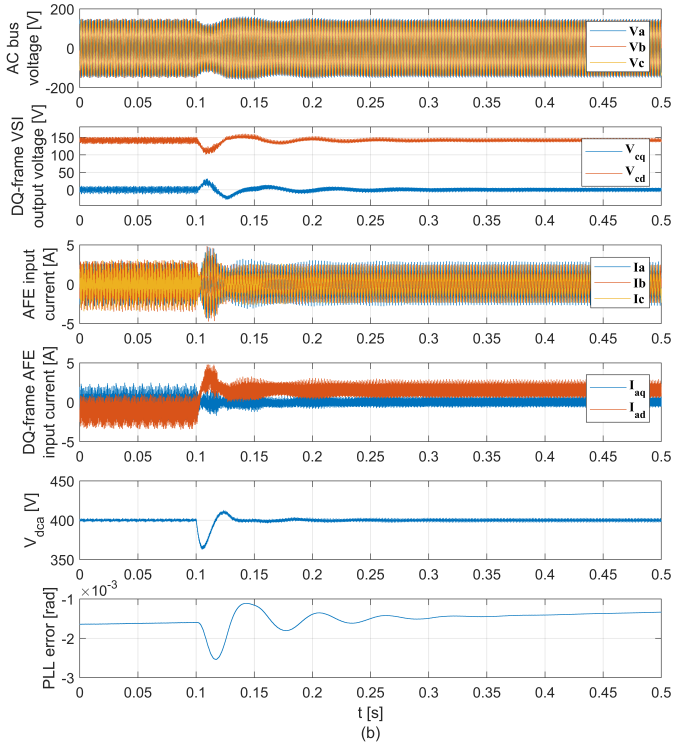

(a)

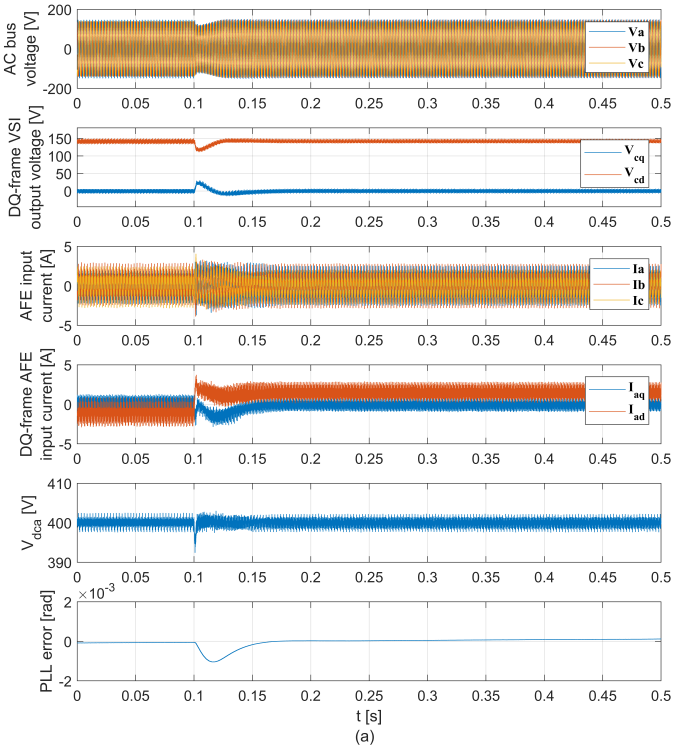

(b)

Fig. 6. Dynamic response waveforms of (a) traditional PI controller and (b) optimal H2 controller, under 0.8kw step load change

TABLE I
PARAMETERS OF EXPERIMENTAL RIG

VSI			
R	$300m\Omega$	V_{dc}	$290V$
L	230μH	V_{cdref}	$141V$
C	33μF	V_{cqref}	$0V$
AFE			
R_a	$800m\Omega$	P	0.8kW
L_a	565μH	V_{dcaref}	$400V$
C_a	100μF	I_{aqref}	$0A$

TABLE II
PARAMETERS OF VSI PI CONTROLLER

	Voltage loop	Current loop
Higher bandwidth	0.037+10.552/s	2.301+7354.8292/s
Lower bandwidth	0.016+2.084/s	0.856+1452.805/s

and its voltage bandwidth is $f_v = 23$Hz. Then two different controllers for AFE were synthesised by the method stated in III-A and III-B, and denoted as traditional PI controller and optimal H2 controller respectively. AFE adopting these two controllers are each powered by the fixed VSI. A transient is created by suddenly loading the constant power load $P = 0.8$kW, at t=0.1s in Fig.6. The dynamic responses on the grid and AFE DC-link when these two controllers are adopted respectively are shown in Fig.6(a) and (b).

Optimal H2 controller tuned including identified model has a transient time of 0.05sec whereas 0.15sec of traditional PI controller. The undershoot on AFE DC-link voltage V_{dca} also shows a great advantage, 0.019 p.u. of optimal H2 controller contrasting with 0.09 p.u. of PI controller, shown in Fig.7. Note that the traditional PI controller here is already tuned with the fastest possible speed by the PI control scheme in Fig.4. Its PI gains are $K_{pv} = 0.062$, $K_{iv} = 9.869$,$K_{pi} = -6.299$ and $K_{ii} = -22305.305$.

B. Case with Lower Bandwidth VSI

Furthermore, to explore the capability of optimal H2 controller, the voltage bandwidth of VSI is decreased to $f_v = 4.8$Hz, corresponding to the 3rd row in Table.II. This means bigger output impedance of VSI and reduced stability margin, and more serious challenge for AFE design [11].

In this case, the optimal H2 controller could still stabilize the system under the load change (Fig.7(c)) while traditional PI controller could not (Fig.7(d)). In the meantime, characteristic loci derived from impedance ratio matrix of the two subsystems are plotted in Fig.8. As can be seen, the loci of H2 optimal controller (red curve) are further from critical point $-1 + 0i$, which means a larger stability margin [2]. When the VSI decreased its bandwidth (Fig.8(b)), the loci of PI (blue dash curve) are too close to $-1 + 0i$ and it is not sufficient to maintain stability under network disturbances. It corresponds to the fact in Fig.7(d) that instability is yielded. In all, the optimal controller considering the identified grid is much better in mitigating interactions and extending stability margin of the whole grid.

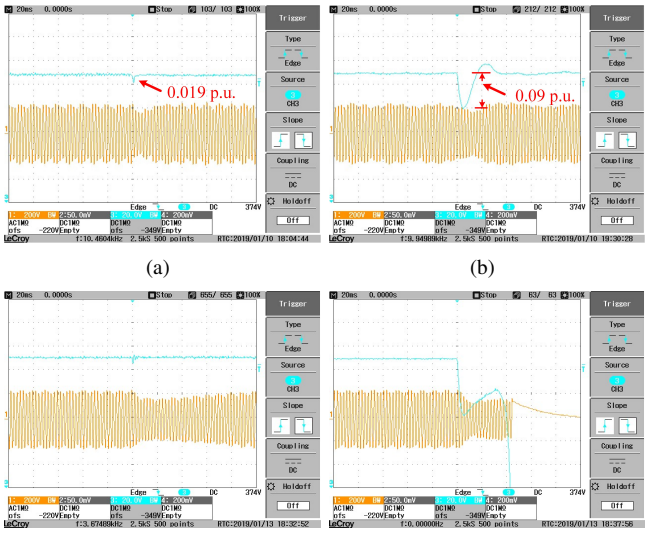

Fig. 7. AFE DC-link voltage (light blue) and phase-to-phase grid voltage (yellow) on scope — (a) optimal H2 controller, high bandwidth VSI (b) PI controller, high bandwidth VSI (c) optimal H2 controller, low bandwidth VSI (d) PI controller, low bandwidth VSI

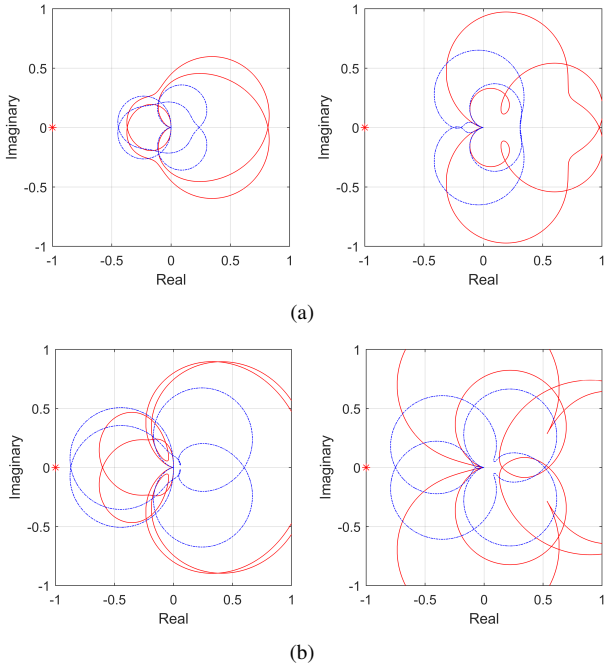

Fig. 8. Characteristic loci of optimal H2 controller (red) and PI controller (blue), each converter have 2 loci (λ1 in left figure and λ2 in right figure) — (a) high bandwidth VSI (b) low bandwidth VSI

V. Conclusion

This work proposes the use of a system impedance estimation seen at the PCC of the active front-end under study in order to identify an equivalent system model and then using structured h2 optimization algorithms to synthesize an optimal controller. A perturbation injection method is used for impedance measurement, while subspace identification and PEM algorithms are applied to identify a state space model of the unknown grid side. The method has been demonstrated for a simplified two-converter system. Experimental results clearly show that when the identified model of the unknown converter is taken into account, the controller derived from the established overall model gives more stability margin and better dynamic performance.

References

[1] X. Roboam, B. Sareni, and A. De Andrade, "More electricity in the air: Toward optimized electrical networks embedded in more-electrical aircraft," *IEEE industrial electronics magazine*, vol. 6, no. 4, pp. 6–17, 2012.

[2] B. Wen, D. Dong, D. Boroyevich, R. Burgos, P. Mattavelli, and Z. Shen, "Impedance-based analysis of grid-synchronization stability for three-phase paralleled converters," *IEEE Transactions on Power Electronics*, vol. 31, no. 1, pp. 26–38, 2016.

[3] A. A. A. Radwan and Y. A. I. Mohamed, "Modeling, analysis, and stabilization of converter-fed ac microgrids with high penetration of converter-interfaced loads," *IEEE Transactions on Smart Grid*, vol. 3, no. 3, pp. 1213–1225, 2012.

[4] L. Asiminoaei, R. Teodorescu, F. Blaabjerg, and U. Borup, "A new method of on-line grid impedance estimation for pv inverter," in *Nineteenth Annual IEEE Applied Power Electronics Conference and Exposition, 2004. APEC '04.*, vol. 3, Feb 2004, pp. 1527–1533 Vol.3.

[5] K. Li, D. Dewar, A. Formentini, P. Zanchetta, and P. Wheeler, "Optimized control design for power converters in power electronics embedded networks integrating grid model identification," in *2018 IEEE Industry Applications Society Annual Meeting (IAS)*, Sep. 2018, pp. 1–6.

[6] D. Dewar, A. Formentini, and P. Zanchetta, "Automated and scalable optimal control of three-phase embedded power grids including pll," in *2017 IEEE Energy Conversion Congress and Exposition (ECCE)*, Oct 2017, pp. 4252–4259.

[7] J. Alvarez-Ramirez, I. Cervantes, G. Espinosa-Perez, P. Maya, and A. Morales, "A stable design of pi control for dc-dc converters with an rhs zero," *IEEE Transactions on Circuits and Systems I: Fundamental Theory and Applications*, vol. 48, no. 1, pp. 103–106, Jan 2001.

[8] D. Dewar, K. Li, A. Formentini, P. Zanchetta, and P. Wheeler, "Performance analysis of h_2 optimally controlled three-phase grids," 09 2018, pp. 2258–2264.

[9] D. Arzelier, D. Georgia, S. Gumussoy, and D. Henrion, "H2 for hifoo," *arXiv preprint arXiv:1010.1442*, 2010.

[10] A. G. Costa, J. L. B. Maldonado, F. A. Romero, J. C. Sanmartín, M. Valarezo, and H. Castillo, "N4sid method applied to obtain a discrete-time linear state space system as a mathematical model of a jaw crusher prototype," in *2017 CHILEAN Conference on Electrical, Electronics Engineering, Information and Communication Technologies (CHILECON)*, Oct 2017, pp. 1–6.

[11] B. Wen, D. Boroyevich, R. Burgos, P. Mattavelli, and Z. Shen, "Analysis of dq small-signal impedance of grid-tied inverters," *IEEE Transactions on Power Electronics*, vol. 31, no. 1, pp. 675–687, 2016.